JOURNAL OF MATERIALS SCIENCE 32 (1997) 5313–5319

Lubricious zinc oxide films: synthesis, characterization and tribological behaviour

J. S. ZABINSKI*, J. CORNEILLE, S. V. PRASAD
Materials Directorate, Wright Laboratory (WL/MLBT), Wright-Patterson Air Force Base, OH 45433, USA

N. T. McDEVITT
RAMSPEC Research, 4399 E. Mohave Drive, Dayton, OH 45431, USA

J. B. BULTMAN
University of Dayton Research Institute, Wright Laboratory, Wright-Patterson Air Force Base, OH 45433, USA

Solid lubricants that are effective over an extreme range of operating temperatures are necessary for the development of new generation high-performance gas turbine engines with increased propulsion capability. While oxides have the potential to perform as high-temperature lubricants, they typically have high friction and create abrasive wear debris at low temperature. The objective of this work was to create oxides that have good tribological properties at room temperature through control of microstructure and stoichiometry. Zinc oxide films were grown by pulsed-laser deposition. The stoichiometry and microstructure of the films were controlled by adjusting substrate temperature and oxygen partial pressure during pulsed-laser deposition. Chemistry and microstructure were probed using SEM, X-ray diffraction, X-ray photoelectron spectroscopy and Raman spectroscopy. Friction coefficients and wear life were measured using a ball-on-flat tribometer. The degree of similarity of the coatings to bulk ZnO was RT, vac $<$ RT, O_2 $<$ 300 °C, vac $<$ 300 °C, O_2. Coatings with oxygen deficiency and nanoscale structure have low friction (i.e. $\mu < 0.2$) and long wear lives (i.e., greater than 10^6 cycles) at room temperature. As the chemistry and crystal structure of a coating approaches that of bulk ZnO, its tribological properties degrade and can become load/speed sensitive. An important result of this study is that oxides can be made to provide good tribological properties at room temperature. Thus, there is significant potential to produce low-friction, low-wear oxide coatings for wide-temperature range applications by controlling nanostructure and oxygen vacancies.

1. Introduction

Lubricants that are effective over an extreme range of operating temperatures are necessary for the development of new-generation high-performance gas turbine engines with increased propulsion capability. If suitable lubricant materials were available, engines could be run at higher temperatures and therefore more efficiently. Unfortunately, there is no single lubricant that can provide low friction over the desired range, from subambient to 800 °C. Liquids and polymers can only function in moderate temperature regimes. The well-known solid lubricants, such as graphite and molybdenum disulfide (MoS_2), oxidize in air at temperatures above 400 or 450 °C and thereby lose their lubricating properties. In humid environments, oxidation reduces the wear life of MoS_2 even at room temperature.

A compilation of lubricant materials by McMurtrey reveals that most solid lubricant formulations consist of MoS_2 or graphite [1]. For high-temperature applications, WS_2 is sometimes used because it has been reported to have an upper operating temperature limit of about 100 °C higher than that of MoS_2. Lead oxide provides lubrication in the temperature range from 450–650 °C, and CaF_2/BaF_2 provides low friction above about 700 °C. After considering the lubricants available, it is apparent that spanning a large temperature range is a challenge. For the most part, few new high-temperature lubricants or lubricant systems have been reported. There are several notable exceptions:

* Author to whom all correspondence should be addressed.

0022–2461

(1) adaptive lubricants, which are materials whose properties change with increasing temperature to maintain low friction [2, 3], (2) caesium and zinc thiomolybdates and thiotungstates [4], (3) TiO_x materials specially formulated to have oxygen deficiencies and, therefore, mechanically weak shear planes [5, 6] and (4) oxides and double oxides [7, 8]. While oxides have the potential to perform as high-temperature lubricants, they typically have high friction and create abrasive wear debris at low temperature. If oxides could be made to have good tribological properties at room temperature, they could solve many problems requiring wide temperature range lubricants.

Many oxides are stable in air at high temperatures. However, their behaviour as thin-film solid lubricants has not been extensively investigated because they are typically brittle. Their inability to deform plastically or shear easily hinders them from forming smooth friction-reducing third-body films on wear surfaces. In addition, the wear debris from an oxide is usually abrasive. Birringer and co-workers [9, 10] presented a new approach to overcome brittleness in ceramic materials. They reported that conventionally brittle polycrystalline ceramics could become ductile if their grain size is reduced to a few nanometres. The nanocrystalline material could permit large plastic deformation at low temperatures. The strain-rate sensitivity of a nanocrystalline ceramic is usually much higher than that of a single-crystal material, and the value of the strain-rate sensitivity increases as the grain size is decreased [11]. For instance, the strain-rate sensitivity of nanophase TiO_2 has been reported to be a quarter of that of lead at room temperature, indicating a potential for significant ductility in these oxide ceramics [11].

Gardos [5, 6] proposed an alternative mechanism for turning oxides, particularly substoichiometric rutile (TiO_{2-x}), into lubricants. Gardos hypothesized that the energetics, including bond-length changes, which depend on electronic properties associated with vacancies in the lattice, are ultimately responsible for variations in shear strength. Control of grain size and/or stoichiometry may permit normally brittle oxides to become useful solid lubricants at low temperatures. Oxides have already been shown to be lubricious at elevated temperatures. Therefore, the development of a ductile/lubricious oxide coating for mechanical elements would be a major breakthrough in lubrication over a wide temperature range.

The purpose of this work was to explore, using pulsed-laser deposition (PLD), the activation of the nanocrystalline and defect mechanisms for producing low-friction behaviour in oxides. It has already been demonstrated that PLD is a viable technique for controlling crystallinity and stoichiometry in solid lubricant thin films [12]. Here, the synthesis, characterization, and preliminary tribological behaviour of thin-film coatings of zinc oxide grown by PLD are reported.

The tribological properties of ZnO powders were evaluated around 1960, but the data did not generate much research activity [7, 8]. Reported values of friction coefficient at 704 °C were around 0.3 at steady state. ZnO melts at 1970 °C. Considering these properties, ZnO was selected for further research as a thin-film solid lubricant with the intention of using PLD to adjust film microstructure and stoichiometry. Although ZnO has been grown by a variety of techniques, including PLD [13, 14], no systematic tribological study of well-characterized thin films has been reported. In the current study, several permutations of deposition conditions, namely the substrate temperature and oxygen partial pressure, were employed to grow films with different crystal size and oxygen content.

2. Experimental procedure

2.1. Pulsed-laser deposition

The system used for pulsed-laser deposition is constructed from a stainless steel vacuum chamber that was specially instrumented for PLD and magnetron sputtering, and is shown in Fig. 1. There are four key components: (1) a laser, (2) optical beam steering and focusing, (3) an instrumented chamber, and (4) a computer data collection and process control system. For the experiments discussed in this manuscript, a Lambda Physik LPX 110i excimer laser was filled with a Ne, KrF mixture to provide a beam of ultraviolet radiation at 248 nm. The beam was pulsed at a rate of 10 Hz (17 ns pulse width) and it was focused to a 2.0 by 4.0 mm rectangle on the target face providing a fluence of about 2.0 $J\,cm^{-2}$. Beam steering was accomplished using a computer-controlled raster mirror. The beam was brought into the deposition system through an MgF_2 window and directed toward the target. Film uniformity was maximized by (1) rotating the target and the substrate during deposition, and (2) rastering the laser beam across the target under computer control. Targets were polished prior to each deposition to minimize roughness and increase deposition rates; they were cleaned in vacuum using the laser with the sample shutter closed. Deposition was commenced by opening the shutter. The base pressure in the chamber was 9×10^{-7} Pa. A calibrated quartz crystal oscillator was used to measure film thickness. Resistive heating was employed to degas and/or

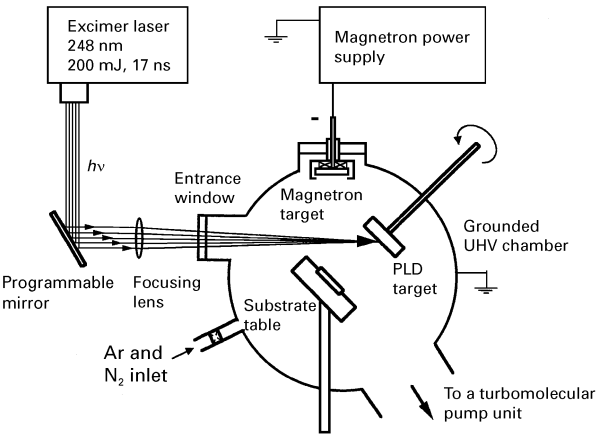

Figure 1 Schematic drawing of the PLD system.

TABLE I Deposition parameters for ZnO film. RT = room temperature

	Temp. (°C)	O_2 pressure (Pa)
RT, vac	RT	9×10^{-7}
RT, O_2	RT	6.7×10^{-1}
300 °C, vac	300	9×10^{-7}
300 °C, O_2	300	6.7×10^{-1}

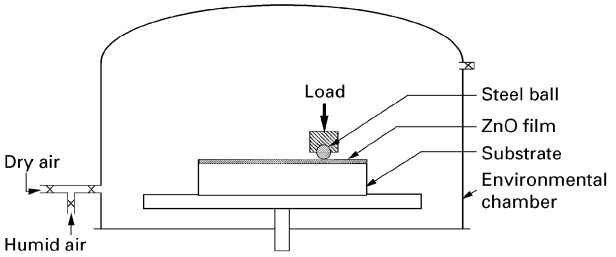

Figure 2 Schematic drawing of the tribometer.

anneal the specimens; temperature was measured using a calibrated infrared pyrometer. Reactive gases were input to the system through a leak valve and pressure was monitored using a capacitance manometer. At high vacuum, pressure was measured by a Bayert Alpert gauge. System parameters were monitored using a computer: film thickness, growth rate, system pressure, laser power, laser pulse rate, and residual gas concentrations.

The major objective of this research was to grow oxide films with different stoichiometries and varying degrees of crystallinity. In order to achieve this objective, four different deposition conditions were employed, as listed in Table I. A commercial hot-pressed ZnO disc (99.9% purity, hexagonal crystal structure), obtained from Cerac Inc., was used as the target material.

2.2. Sample preparation and analysis

Substrates were fabricated from 440C stainless steel (SS) coupons that were polished to 1 μm. Materials were cleaned in soap and water and then ultrasonically washed in acetone and methanol.

Surface chemistry was studied with a Surface Science Instruments (SSI) M-probe XPS instrument operated at a base pressure of 3×10^{-7} Pa. Using an aluminium anode, a 400×1000 μm line spot, and a 25 eV pass energy, the full-width at half-maximum (FWHM) of the Au $4f_{7/2}$ peak was 0.71 eV. Binding energy positions were calibrated against the Au $4f_{7/2}$ peak and energy separations were calibrated using the Cu 3s and Cu $2p_{3/2}$ peaks at 122.39 and 932.47 eV, respectively. Bulk chemistry and film crystallinity were investigated by Raman spectroscopy using a SPEX 1877 spectrometer and the incident light of a 514.5 nm Ar^+ laser. An intensified 1024 element, diode array detector was used to collect the Raman signal. Crystal structures were determined using data acquired by a Rigaku D/max-1B diffractometer equipped with a thin film attachment and a monochromator. High-resolution scanning electron microscopy (SEM) was performed on the films using a Leica 360 field emission SEM equipped with an energy dispersive X-ray analyser.

Room-temperature friction and wear data from coated specimens were collected using a ball-on-flat tribometer run with the specimens in the horizontal position as shown in Fig. 2. The ball was held in a lever arm, and the friction force was measured using strain gauge circuitry. The normal load was computed from the dead weight hung in the cantilever assembly. In order to maintain a constant humidity level in the test environment, the ball–disc assembly was enclosed in a chamber. Flow rates of dry air and saturated humid air were adjusted to control relative humidity (RH) from near zero to almost 100%. The percentage relative humidity was measured by a high-performance sensor inserted in the chamber. A 3.125 mm diameter 440C steel ball was used as the counterface. For each friction track, the rotational speed was adjusted to get a constant sliding speed of 50 mm s^{-1}. The majority of the friction measurements were made at a normal load of 1 N. For steel-on-steel, a normal load of 1 N on a 3.125 mm diameter ball corresponds to a Hertzian contact pressure of 675 MPa. The relative humidity in the current study was maintained at 50%, and measurements were made at room temperature.

3. Results

Surface chemistry and stoichiometry were determined from analyses of the Zn $4f_{5/2-7/2}$ and O 1 s XPS spectra and Zn *LMM* Auger line. The ZnO target underwent charging and an electron flood gun was used to neutralize the surface. Peak positions in this instance were referenced to adventitious carbon. Peaks were fitted to Voight functions by minimizing the chi-squared value; binding energies, and Zn/O atomic ratios determined from the fitted data and are presented in Table II. Carbon and oxygen contamination were present on the surface of all specimens due to handling in air. Crystal structure and the degree of crystallinity were determined by analysis of Raman spectra and glancing angle X-ray diffraction (GAXRD) which are shown in Figs 3, 4 and Table III.

A high-resolution scanning electron micrograph of the RT, vac film is shown in Fig. 5a. The film is extremely smooth and no grain boundaries could be seen even at very high magnification. By comparison, the RT, O_2 films begin to reveal some structure (Fig. 5b). Introduction of oxygen has resulted in the formation of nanophase clusters. Also, compared with the films grown in vacuum, those grown in partial oxygen appear to be rough. Fig. 5c is a typical high-resolution scanning electron micrograph of 300 °C, vac films. Unlike the previous ones, the topography of the 300 °C, vac film appears to be granular with nanocrystalline grains. A typical scanning electron micrograph of 300 °C, O_2 films is shown in Fig 5d. Here, the surface exhibited a granular structure.

TABLE II XPS data from the different films. Binding energies ± 0.04 eV; atomic ratios ± 0.03

	O 1s (eV)	Zn $2p_{3/2}$ (eV)	Zn *LMM* (eV)	O/Zn
ZnO target	531.28	1023.46	987.30	1.0
RT,vac	531.31	1022.48	987.60	0.75
RT, O_2	531.30	1023.60	987.76	0.95
300 °C, vac	531.25	1023.44	987.14	0.90
300 °C, O_2	531.26	1023.45	987.40	0.95

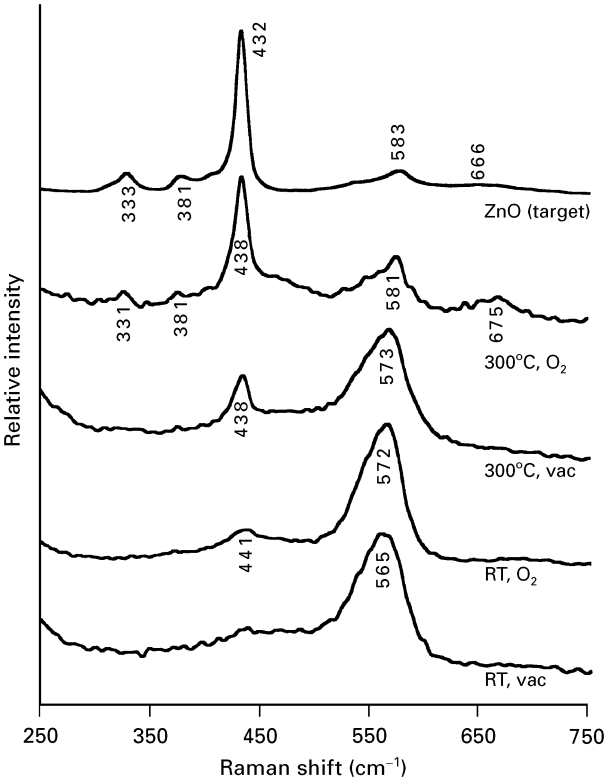

Figure 3 Raman spectra of the ZnO target and the different films.

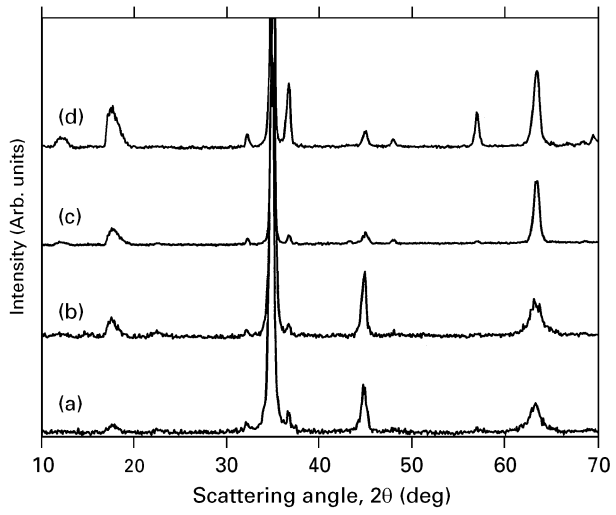

Figure 4 X-ray diffraction patterns from the different films: (a) RT, vac, (b) RT, O_2; (c) 300 °C, vac; (d) 300 °C, O_2.

The grains are mostly smaller than 100 nm, but the microstructure appears to be fully crystalline. This observation is supported by the Raman data presented below.

The steady-state coefficient of friction (COF) for the polished surface of the hot-pressed ZnO (stoichiometeric, hexagonal) is rather high, 0.65. Friction coefficients for the different films are reported in Table IV. A typical friction trace for the RT, O_2 film is shown in Fig. 6. As can be seen, there is a short wear-in period and then a smooth trace with $\mu = 0.16$ is generated for the remainder of the 10 000 cycle test. The RT, vac and 300 °C, vac films also had short run-in periods followed by a steady-state regime. However, the friction trace from the 300 °C, O_2 (Fig. 7) showed several peaks in the early portion of this trace, and the COF varied between 0.2 and 0.4.

4. Discussion

4.1. Film chemistry and microstructure

X-ray photoelectron spectroscopy (XPS), Raman, and X-ray diffraction (XRD) data were used to study the film chemistry and crystallinity. All films were slightly oxygen deficient. Sputter etching the films for 10 s, 5 and 15 min did not significantly change their stoichiometries, demonstrating that they did not suffer post-deposition oxidation. All peaks in the XRD scans were accounted for by hexagonal ZnO and the 440C substrate. Raman data provided much greater insight into the degree of perfection of the ZnO chemistry and crystal structure as compared to the target material than XRD.

The RT, vac films were the most oxygen deficient; the stoichiometry, determined using XPS data, $ZnO_{0.75}$. The oxygen deficiency is likely caused by recombination of oxygen atoms in the plasma or at the film surface and subsequent removal of the O_2 molecule through the pumping system. A comparison of the Raman spectra from the four films to that from the hot-pressed hexagonal ZnO target is shown in Fig. 3. The target material has bands at 333, 381, 432, 583 and 666 cm^{-1} with the most intense band at 431 cm^{-1}. The Raman spectrum from the RT, vac film shows the most intense peak is at 565 cm^{-1}. It should be noted that: (1) it is about 18 cm^{-1} less than the corresponding target peak, and (2) the corresponding target peak is of quite low intensity. Unambiguous identification of the origin of this peak has not been made, although it is likely related to the crystal size, orientation, and/or oxygen deficiency in the film. The dominance of the (0 0 2) line in the XRD scans suggests a texture with the *c*-axis preferentially aligned perpendicular to the substrate. The width of the (1 0 3) peak was somewhat broadened. This suggests limited spatial extent or a distribution of *d*-spacing. The topography of the film is smooth, and the high-resolution scanning electron micrographs did not show any grain boundaries.

To increase the oxygen content of the film, the deposition chamber was backfilled with oxygen to a pressure of 6.7×10^{-1} Pa while keeping the substrate at room temperature. Background oxygen increased the oxygen content of the film ($ZnO_{0.95}$) compared to those grown in vacuum ($ZnO_{0.75}$). The Raman spectrum shows that the 572 cm^{-1} peak is still dominant and that the films are very similar to the RT, vac films.

TABLE III XRD data from the different films

ZnO powder			RT, vac		RT, O_2		300 °C, vac		300 °C, O_2	
d (nm)	I/I_0	($h\,k\,l$)	d (nm)	I/I_0	d (nm)	I/I_0	d (nm)	I/I_0	d (nm)	I/I_0
0.2816	71	1 0 0	0.2780	3	0.2784	3	0.2781	2	0.2785	4
0.2602	56	0 0 2	0.2576	100	0.2569	100	0.2572	100	0.2576	100
0.2476	100	1 0 1	0.2449	6	0.2446	4	0.2451	3	0.2455	18
0.1911	29	1 0 2	–	–	–	–	0.1899	1	0.1898	3
0.1626	40	1 1 0	–	–	–	–	0.1616	1	0.1617	10
0.1477	35	1 0 3	0.1469	9	0.1471	10	0.1469	16	0.1469	21

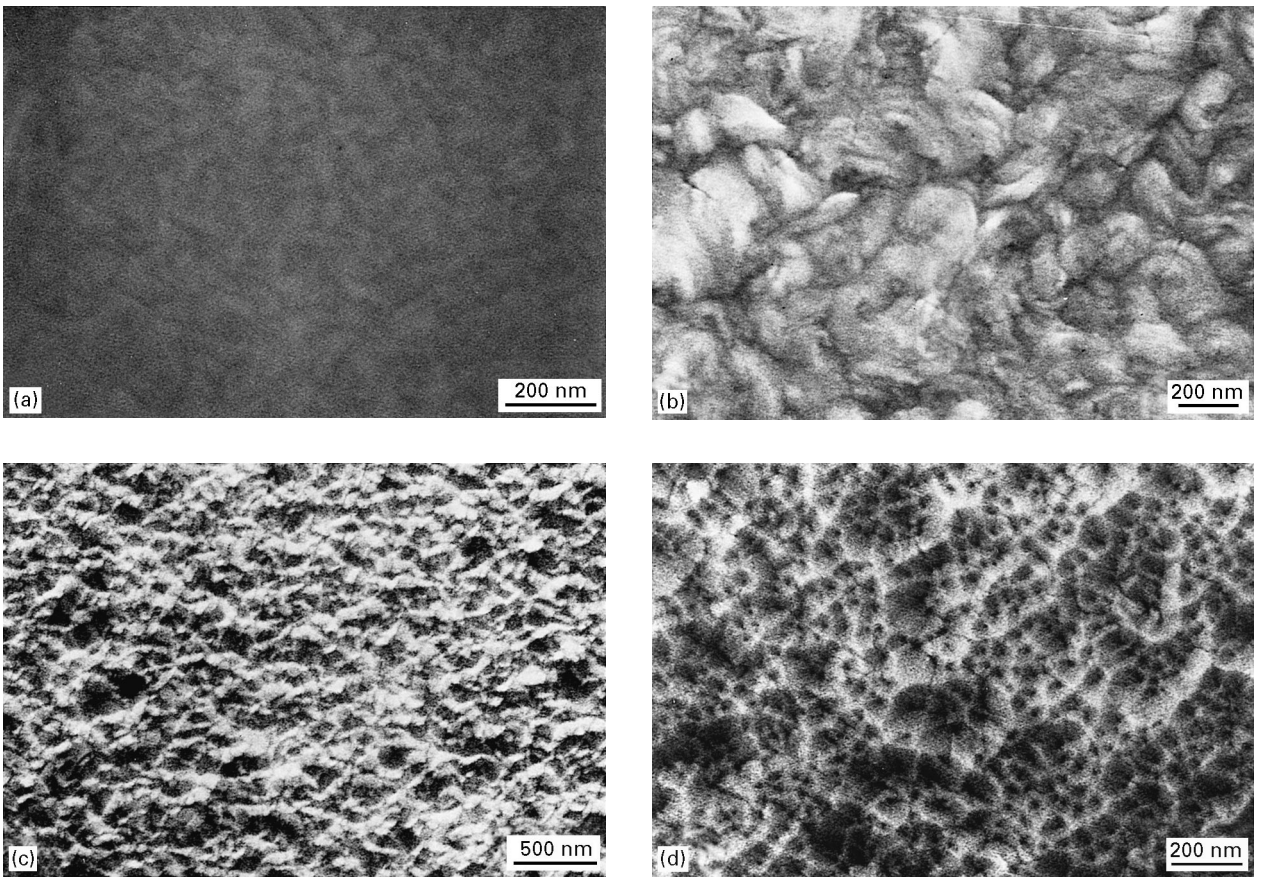

Figure 5 SEM images from the different films: (a) RT, vac, (b) RT, O_2; (c) 300 °C, vac; (d) 300 °C, O_2.

TABLE IV Friction coefficients for ZnO films. SS = steady state after 10 000 cycles

	$\mu_{initial}$	μ_{ss}
RT, vac	0.6	0.34
RT, O_2	0.1	0.16
300 °C, vac	0.1	0.18
300 °C, O_2	0.2	0.3

It is noted that the RT, O_2 films are somewhat more similar to the target material because the peak at 441 cm^{-1} corresponding to the dominant target peak, was slightly more defined. The relative peak intensities and peak widths in the XRD scans did not significantly change indicating a similar texture and crystal dimension compared to the RT, vac film. However, high-resolution SEM examination revealed the presence of nanoscale structure in the RT, O_2 films (Fig. 5b).

To increase the grain growth and the oxygen content further, the substrate temperature was raised to 300 °C while maintaining the vacuum. XPS data indicated that the film was quite similar to those grown at room temperature and were $ZnO_{0.90}$. The Raman peak at 438 cm^{-1} was significantly more pronounced and sharper for the 300 °C, vac film than for the previous films, suggesting it is more similar to the crystalline target material. However, the 573 cm^{-1} peak was still dominant. The (0 0 2) peak in the XRD scan was still dominant; however, the relative peak intensities changed somewhat, indicating a change in film texture. Specifically, the (1 0 3) peak grew in relative intensity but it still remained broadened. It is

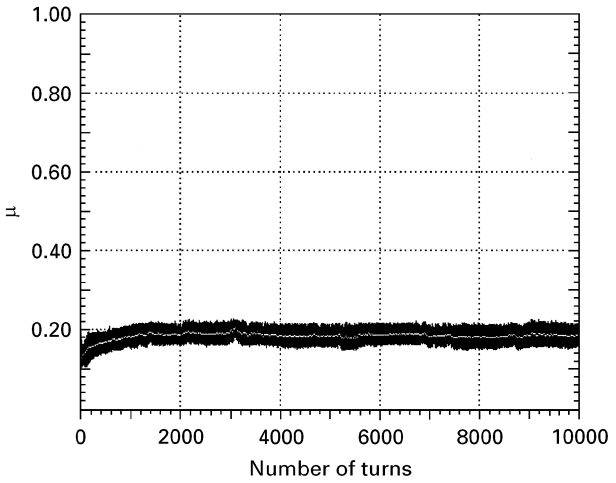

Figure 6 Friction trace from the RT; O_2 film.

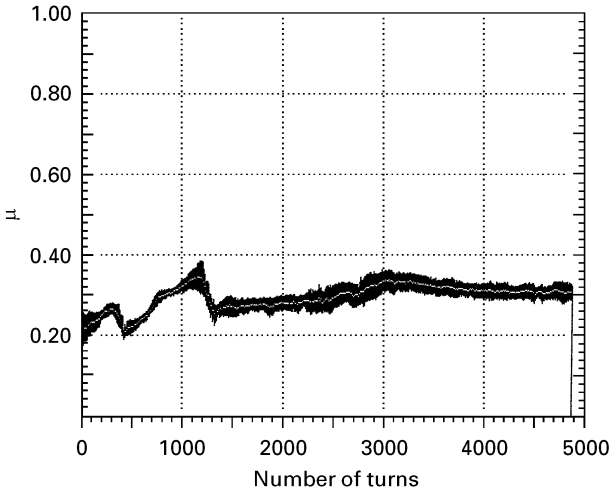

Figure 7 Friction trace from the 300 °C, O_2 film.

worth noting that the topography of the 300 °C, vac film is granular with nanocrystalline grains.

The films grown in an oxygen background (i.e. 6.7×10^{-1} Pa) at 300 °C were $ZnO_{0.95}$. Among the various films grown under four sets of conditions, Raman spectra from the 300 °C, O_2 films best match with that of the target material. The peak at 438 cm^{-1} became dominant as for the ZnO target. In addition, peaks at 331, 381, 581 and 675 cm^{-1} closely match the position and relative intensity of corresponding target peaks. XRD peak intensity ratios changed significantly with the (1 0 3) and (1 0 1) peaks becoming more intense, indicating a change in the texture. Peak widths remained relatively unchanged. The micrographs of the 300 °C, O_2 films reveal dark and light areas. The contrast in the 300 °C, O_2 films may be caused by a different chemistry or crystal structure or by topography. However, XPS, Raman, or energy-dispersive X-ray spectroscopy cannot be used to probe the regions separately because the probing radiation is large compared to the size of the contrast. However, we believe the contrast is most likely caused by shadowing associated with the topography of the grains.

In summary, the films are all crystalline based on XRD data but Raman data best show their degree of similarity (perfection) to the target material: RT vac < RT, O_2 < 300 °C, vac < 300 °C, O_2. The films are oxygen deficient with the RT, vac film having the lowest oxygen concentration. SEM data clearly show nanophases/nanostructure in the RT, O_2 and 300 °C, vac films.

4.2. Film tribology

The results of the current study clearly demonstrate that the friction coefficients of pulsed-laser-deposited ZnO films, particularly RT, O_2 and 300 °C, vac are comparable to that of commonly used solid lubricants, like graphite. It is noted that the friction coefficient of hot-pressed ZnO is rather high, 0.65. Zinc oxide, either in powder form or as a compacted disc, does not provide a lubricious surface, whereas nanophase/nanostructured oxygen-deficient ZnO coatings deposited by PLD provide lubricious surfaces with friction coefficients of less than 0.2.

Among the various PLD ZnO films, the RT, O_2 and 300 °C, vac films had the lowest friction. Interestingly, these two films had nanoscale microstructural features. For instance, the RT, O_2 film had clusters which are of 50–60 nm in size, and the 300 °C, vac film had a granular structure with an extremely fine grain size. This film performed the best, so it was further evaluated by conducting a long-duration tribo test. The wear life of a 0.5 μm thick RT, O_2 film was nearly a million cycles, and for most of the test, the COF was less than 0.2. Because plastic deformation in nanocrystalline films can be strain-rate sensitive, several combinations of load and speed were used during the test. However, the changes had no significant effect on the friction behaviour after the steady-state regime was reached [15].

Finally, the 300 °C, O_2 film showed variation in friction during the run-in period and had the highest steady-state friction. Surprisingly, when the contact stress was reduced from 675 MPa to 425 MPa by increasing the ball diameter to 6.25 mm, the COF rose to over 0.7 and the big fluctuations in the friction force disappeared. The Raman spectrum of this film most closely resembles that of the target indicating the onset of a microstructure with a sufficiently large bulk-like phase. Adjusting the microstructure further toward that of the target is clearly undesirable.

It is well established that the plastic deformation of crystalline solids occurs by the movement of lattice dislocations and/or by diffusional creep. In the case of oxides the lattice dislocations are usually immobile, and plastic deformation by diffusional creep is significant only at temperatures close to the melting point. That is why the friction coefficient of ZnO powder and the hot-pressed ZnO disc were found to be high. However, reducing the grain size of ceramics to nanometre levels may allow plastic flow by diffusional creep even at room temperature [9]. The enhancement of dislocation movement caused by the oxygen vacancies is also possible. SEM examination of the wear scars revealed that RT, O_2 films show a

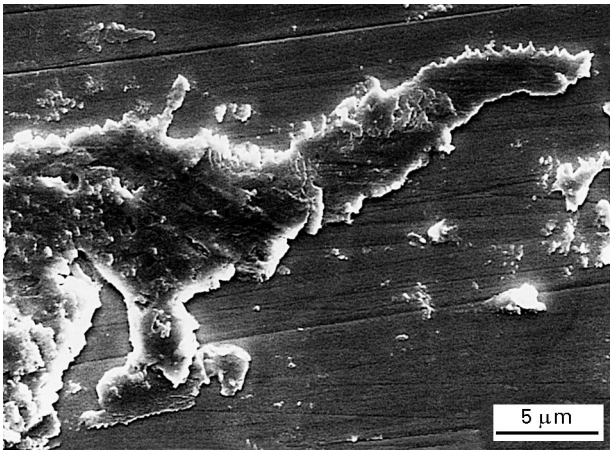

Figure 8 SEM image of plastic deformation in the wear track of the RT, O_2 film.

significant amount of plastic deformation. A typical micrograph showing heavy deformation is presented in Fig. 8. The relative contributions and interactions of grain size and stoichiometry to tribological properties require further investigation. The results presented in this study demonstrate that oxides can be made to have good tribological properties at room temperature. Because ZnO is known to have good tribological properties at elevated temperature, the potential of ZnO as a candidate wide temperature range solid lubricant warrants further study.

5. Conclusions

The stoichiometry and microstructure of ZnO films can be controlled by adjusting substrate temperature and oxygen partial pressure during pulsed-laser deposition. The degree of similarity of the films to target material based on Raman spectra was RT, vac < RT, O_2 < 300 °C, vac < 300 °C, O_2. Films with oxygen deficiency and nanoscale structure have low friction (i.e. $\mu < 0.2$) and long wear lives (i.e. greater than 10^6 cycles). As the chemistry and crystal structure of a film approaches that of bulk ZnO, its tribological properties degrade and can become load/speed sensitive. An important result of this study is that oxides can be made to provide good tribological properties at room temperature. Thus, there is significant potential to produce low-friction, low-wear oxide coatings for wide temperature range applications by controlling nanostructure and oxygen vacancies.

References

1. E. L. McMURTREY, NASA TM-86556 (George C. Marshall Space Flight Center, NASA, Huntsville AL, 1985).
2. J. S. ZABINSKI, S. V. PRASAD and N. T. McDEVITT, in "Proceedings of the 82nd NATO/AGARD *Tribology of Aerospace Systems Specialist Meeting*", Sesimbra, Portugal, 6–7 May 1996, NATO, London, AGARD CP-589 (1996) 3.
3. J. S. ZABINSKI, M. S. DONLEY, V. J. DYHOUSE and N. T. McDEVITT, *Thin Solid Films* **214** (1992) 156.
4. J. P. KING and N. H. FORSTER, AIAA Paper 90-2044 presented at the "26th AIAA, SAE, ASME, and ASEE Joint Propulsion Conference", Orlando 16–18 July 1990.
5. M. N. GARDOS, *Tribol. Trans.* **31** (1988) 427.
6. *Idem., ibid.* **33** (1990) 209.
7. M. B. PETERSON and R. L, JOHNSON, *Lubric. Engng* **13**(4) (1957) 203.
8. M. B. PETERSON, S. F. MURRAY and J. J. FLOREK, *ASLE Trans.* **2** (1960) 225.
9. R. BIRRINGER, H. GLEITER, H-P. KLEIN and P. MARQUARDT, *Phys. Lett.* **102A** (1984) 365.
10. J. KARCH, R. BIRRINGER and H. GLEITER, *Nature* **330** (1987) 556.
11. M. J. MAYO, R. W. SIEGEL, A. NARAYANASWAMI and W. D. NIX, *J. Mater. Res.* **5** (1990) 1073.
12. M. S. DONLEY and J. S. ZABINSKI, in "Pulsed-Laser Deposition of Thin Films", edited by D. B. Chrisey and G. K. Hubler (Wiley, New York, 1994) pp. 431–53.
13. N. J. IANNO, L. McCONVILLE, N. SHAIKH, S. PITTAL and P. G. SNYDER, *Thin Solid Films* **220** (1992) 92.
14. V. S. BAN and D. A. KRAMER, *J. Mater. Sci.* **5** (1970) 978.
15. S. V. PRASAD and J. S. ZABINSKI, *Wear* **203–204** 1997) 498.

Received 11 November 1996
and accepted 1 May 1997